



CrossMark
click for updates

Cite this: *RSC Adv.*, 2016, 6, 55382

Facile alkali-assisted synthesis of g-C₃N₄ materials and their high-performance catalytic application in solvent-free cycloaddition of CO₂ to epoxides†

Jie Xu,* Jie-Kun Shang, Quan Jiang, Yue Wang and Yong-Xin Li*

A series of graphitic carbon nitride materials were synthesized using guanidine hydrochloride (GndCl) as a precursor with the aid of alkali treatment. The introduction of alkali successfully enabled GndCl to be transformed into g-C₃N₄ at much lower calcination temperatures (450–475 °C). The g-C₃N₄ samples synthesized under various conditions have been characterized by several techniques including XRD, FT-IR, UV-vis, ¹³C NMR, and XPS spectroscopy. The results confirmed that the alkali could effectively accelerate further condensation of melem-like fragments to g-C₃N₄. Meanwhile, a possible mechanism of alkali-assisted synthesis of g-C₃N₄ from GndCl has been proposed. In solvent-free catalytic cycloaddition of CO₂ to propylene oxide to propylene carbonate (PC), g-C₃N₄-NaOH and g-C₃N₄-KOH materials demonstrated high and stable catalytic performances, affording PC yields of ca. 90% under optimized reaction conditions. Moreover, the activities were superior to those obtained over g-C₃N₄ prepared without alkali treatment. In addition, the catalytic activity along with preparation method for the present g-C₃N₄ has also been compared with other reported g-C₃N₄-based catalysts.

Received 23rd April 2016
Accepted 30th May 2016

DOI: 10.1039/c6ra10509b

www.rsc.org/advances

1. Introduction

Carbon dioxide (CO₂) is the major byproduct of worldwide fossil-fuel-based energy production and is believed to be partly responsible for changes to the global climate.¹ At the present time, carbon capture and storage (CCS) from fossil-fuel power stations is the only strategy being investigated to reduce the emissions of CO₂, however it demands a high cost of energy.² Alternatively, CO₂ is also an abundant, cheap, and sustainable C1 resource.³ In this respect, transformation of CO₂ as a renewable building block to valuable chemicals possesses significant values in both environmental preservation and resource utilization, and therefore has recently become the hot topic both in sustainable chemistry and green catalysis.⁴ Among the various schemes proposed for the transformation of CO₂, because of its high atomic economy, the cycloaddition of CO₂ with epoxides (*e.g.* propylene oxide, PO) to the cyclic carbonates (*e.g.* propylene carbonate, PC), especially performed under solvent-free circumstance, has been considered as the most promising pathway.^{5–7} More importantly, the products of the cycloaddition of CO₂, *i.e.* cyclic carbonates, are also very

significant chemicals, which are extensively used as excellent aprotic polar solvents, electrolytes, fine chemical intermediates, and precursors for polycarbonate materials.^{8,9}

A wide range of catalysts have been explored to promote cycloaddition of CO₂ to cyclic carbonates. Up to now, the ionic liquids (ILs) and organometallic complexes (*e.g.* salen complexes) have been widely recognized as the most efficient catalysts for the reactions.^{6,10} Unfortunately, the crucial issue associated with the application of such catalysts lies in their inherently homogeneous nature, being difficult in product separation and catalyst recovery.^{11,12} Alternatively, immobilization of ILs or metal complexes onto porous solids^{13,14} could practically relieve the above problem. Despite this effort, the high cost of coupling agents and tedious route of immobilization still restrain the further practical implementation of the supported ILs or complexes for catalytic cycloaddition reactions of CO₂.^{15,16} In this context, in terms of both fundamental research and industrial application, it is of significance to search and develop a new solid catalyst that can allow high performance for the catalytic cycloaddition reactions of CO₂.

Very recently, as an analogy of graphite, graphitic carbon nitride (g-C₃N₄) material has been emerged as an appealing and fascinating metal-free material, and attracted a great deal of attention in a wide community.^{17–19} So far, g-C₃N₄ and its based materials have been widely applied in various research fields, including photocatalysis,^{20–22} heterogeneous catalysis,^{23–25} fuel cells,²⁶ gas storage,^{27,28} *etc.* The success of g-C₃N₄ is largely due to its unique combination of multiple physicochemical properties.¹⁷ Of particular note is that g-C₃N₄ has abundant N-

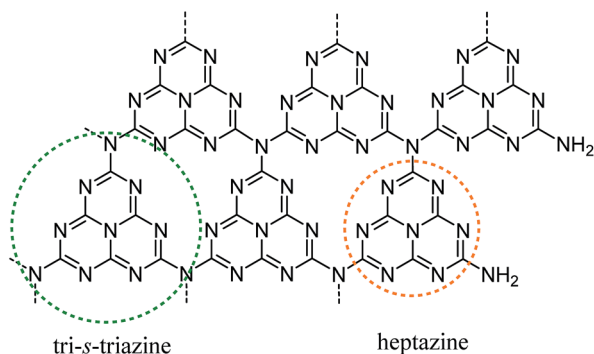
Jiangsu Key Laboratory of Advanced Catalytic Materials and Technology, School of Petrochemical Engineering, Changzhou University, Gehu Road 1, Changzhou, Jiangsu 213164, PR China. E-mail: shine6832@163.com; liyxluck@163.com; Fax: +86-519-86330135; Tel: +86-519-86330135

† Electronic supplementary information (ESI) available: N₂ adsorption–desorption isotherms, surface areas, XPS survey of g-C₃N₄ materials; and FT-IR spectra of the fresh and spent g-C₃N₄ catalysts. See DOI: 10.1039/c6ra10509b

containing species in the forms of amino groups on the edges of graphitic and tertiary amines bridging heptazine rings (Scheme 1); such constitution enables $g\text{-C}_3\text{N}_4$ with a typical solid base.^{16,29} To date, it has been reported that $g\text{-C}_3\text{N}_4$ materials demonstrated potential catalysis in several base-mediated organic reactions, including Knoevenagel condensation^{30–32} and transesterification.^{16,33,34} Moreover, Thomas³⁵ and Park²⁴ *et al.* have found that $g\text{-C}_3\text{N}_4$ materials could effectively activate CO_2 molecules in some CO_2 -involving oxidative reactions. Very recently, Yin *et al.*³⁶ have synthesized phosphorous-modified $g\text{-C}_3\text{N}_4$ materials, and revealed that such $g\text{-C}_3\text{N}_4$ samples could efficiently catalyze the CO_2 cycloaddition to epoxides owing to their acid–base bifunctionality.

Nevertheless, owing to its weak basic intensity, the activity of pristine $g\text{-C}_3\text{N}_4$ materials (namely prepared *via* direct thermal treatment) for the catalytic cycloaddition of CO_2 was indeed limited. To enhance their activity, in our recent work, we have prepared a series of mesoporous $g\text{-C}_3\text{N}_4$ materials, and then loaded them with zinc halides³⁷ or functionalized with quaternary amines.³⁸ Although the modification has successfully improved the final activity of $g\text{-C}_3\text{N}_4$ in the cycloaddition reactions of CO_2 , it should be noted that the mesoporous $g\text{-C}_3\text{N}_4$ materials were fabricated using silica nanoparticles as hard templates *via* a nanocasting method. The preparation process is time-consuming and complicated, meanwhile demanding volatile and toxic HF solution as an etching agent. Furthermore, the employment of such acidic HF solution would neutralize and thus damage the original basic sites of $g\text{-C}_3\text{N}_4$ materials, resulting in an inevitable decline in their catalytic activity.^{16,39}

In continuation of the work, by means of the introduction of transition metal halides into the precursors of $g\text{-C}_3\text{N}_4$, we prepared a series of metal doped bulk $g\text{-C}_3\text{N}_4$, which exhibited enhanced catalytic activities in the transesterification reactions. However, there was potential leaching of metal species. In order to further develop a robust $g\text{-C}_3\text{N}_4$ solid with high-performance activity, in this work, we have introduced a convenient alkali-assisted synthetic approach of $g\text{-C}_3\text{N}_4$, which could be operated under lower thermal treatment temperatures (450–475 °C) compared with the prevailing methods. More encouragingly, the synthesized materials showed high catalytic activities in the solvent-free cycloaddition reactions of CO_2 to epoxides.



Scheme 1 A possible structure of $g\text{-C}_3\text{N}_4$ constituted by the tri-*s*-triazine tectonic units.

2. Experimental

2.1. Preparation of $g\text{-C}_3\text{N}_4$ materials

9 g (0.094 mmol) of guanidine hydrochloride (GndCl) was added into 50 mL of alkali solution (NaOH/KOH) ethanolic solution (0.5 mol L^{-1}), and stirred for *ca.* 2 h under room temperature. During the procedure, white precipitation, *i.e.* alkali metal chloride was observed. The mixture was filtered to remove the precipitation, and the filtrate was dried at 65 °C overnight to evaporate ethanol. Afterwards, the white solid was calcinated from room temperature to the desired temperature with a ramping rate of $3 \text{ }^\circ\text{C min}^{-1}$, and temperate for another 3 h under N_2 atmosphere (20 mL min^{-1}) in a tube furnace. The resultant pale yellow powder was collected and labeled with $g\text{-C}_3\text{N}_4\text{-}T\text{-MOH}$, where MOH and *T* indicated the alkali metal hydroxide and thermal treatment temperature, respectively. For comparison, 9 g of GndCl was directly calcinated without addition of alkali, and the final yellow solid was designated as $g\text{-C}_3\text{N}_4\text{-}T\text{-direct}$.

2.2. Sample characterization

X-ray diffraction patterns were recorded with a Rigaku D/max 2500 PC X-ray diffractometer equipped with a graphite monochromator (40 kV, 40 mA) using Ni-filtered $\text{Cu-K}\alpha$ radiation ($\lambda = 1.5418 \text{ \AA}$).

Fourier transform infrared (FT-IR) spectra of the samples were collected in transmission mode from KBr pellets at room temperature on a Bruker Tensor 27 spectrometer with a resolution of 4 cm^{-1} , using 32 scans per spectrum in the region of $400\text{--}4000 \text{ cm}^{-1}$. The mass ratio of every sample to KBr was constant at 1 : 100.

UV-vis diffuse reflectance spectra (DRS) were recorded on a Shimadzu UV-3600 spectrophotometer. BaSO_4 was used as a standard reference. Each sample was pressed into a thin tablet and tested under ambient conditions. The absorption spectrum was calculated from the reflectance data with Kubelka–Munk function.

X-ray photoelectron spectroscopy (XPS) measurements were performed using a Perkin-Elmer PHI 5000C spectrometer working in the constant analyzer energy mode with $\text{Mg K}\alpha$ radiation as the excitation source. The carbonaceous C 1s line (284.6 eV) was used as the reference to calibrate the binding energies.

The solid-state NMR ^{13}C CP/MAS (cross polarization magic angle spinning) measurement was conducted using a Varian 400WB 300 spectrometer using a 7.5 mm triple-tuned probe spinning at 30 kHz.

Elementary analysis (EA) was performed with Elementar Vario EL III instrument to determine the carbon, nitrogen, and hydrogen contents of the samples.

Nitrogen adsorption–desorption isotherms were measured at $-196 \text{ }^\circ\text{C}$ using a Micromeritics ASAP 2020 analyzer. Before the analysis, the samples were degassed ($10 \text{ }\mu\text{mHg}$) at $150 \text{ }^\circ\text{C}$ for at least 4 h. The specific surface area was calculated according to the Brunauer–Emmett–Teller (BET) method, and pore size

distribution was determined by the Barrett–Joyner–Halenda method.

2.3. Catalytic evaluation

The cycloaddition of CO₂ to PO was carried out in 80 mL stainless steel autoclave equipped with a magnetic stirrer. In a typical reaction process, 10 mL of PO (0.14 mol), 38 mg of ZnI₂ (0.12 mmol), and 0.4 g of the catalyst were added into the reactor. Then, the reactor was pressurized with CO₂ to a desired pressure and heated to 140 °C under stirring for 6 h. After the reaction, the autoclave was cooled down to the room temperature in ice water and the excess of CO₂ was vented. The liquid product was separated by centrifugation and analyzed using a GC equipped with a SE-54 capillary column and FID. The liquid mixture consisted of PO, PC, and 1,2-propylene glycol (PG) as the byproduct originating from the hydrolysis of PO with trace H₂O. No other substance was detected. The carbon balance was nearly 100%. Their quantitative calculation (*i.e.* conversion of PO, and selectivity to PC) was based on an area-normalization method.

The PO conversion and selectivity to PC were calculated as follows:

$$\text{Conv.} = \frac{A_{\text{PC}} \times f_{\text{PC}} + A_{\text{PG}} \times f_{\text{PG}}}{A_{\text{PO}} + A_{\text{PC}} \times f_{\text{PC}} + A_{\text{PG}} \times f_{\text{PG}}},$$

$$\text{Sel.} = \frac{A_{\text{PC}} \times f_{\text{PC}}}{A_{\text{PC}} \times f_{\text{PC}} + A_{\text{PG}} \times f_{\text{PG}}},$$

where A , and f were the peak area of GC, and response factor for each product.

The yield of PC was calculated as

$$\text{Yield} = \text{Conv.} \times \text{Sel.}$$

The TOF (mass of synthesized PC per gram catalyst per hour) for each catalyst was calculated as follows:

$$\text{TOF} = \frac{m_{\text{PC}}}{W_{\text{catal.}} \times t} = \frac{n_{\text{PO}} \times \text{Conv.}\%(\text{PO}) \times \text{Sel.}\%(\text{PC}) \times M_{\text{PC}}}{W_{\text{catal.}} \times t},$$

where n_{PO} , M_{PC} , t , and $W_{\text{catal.}}$ were the molar amount (mmol) of PO, formula weight (g mol⁻¹) of PC, reaction time (h), and the mass of overall catalyst (mg), respectively.

3. Results and discussions

3.1. Structure characterization

Initially, XRD technique was employed to analyze the crystalline structure of g-C₃N₄ materials prepared using various thermal treatment temperatures. As shown in Fig. 1A, when the GndCl precursor was calcinated under low temperatures, *i.e.* 400–425 °C, the corresponding XRD patterns of the synthesized materials demonstrated ternary diffraction peaks in the range of $2\theta = 25$ to 30°, along with some weak peaks below $2\theta = 20^\circ$. The patterns with multiple diffraction lines corresponded to the presence of melem.^{40,41} The presence of melem has also been reported when calcinating dicyandiamide⁴² and melamine⁴⁰ as starting materials under moderate temperatures. Upon elevating the

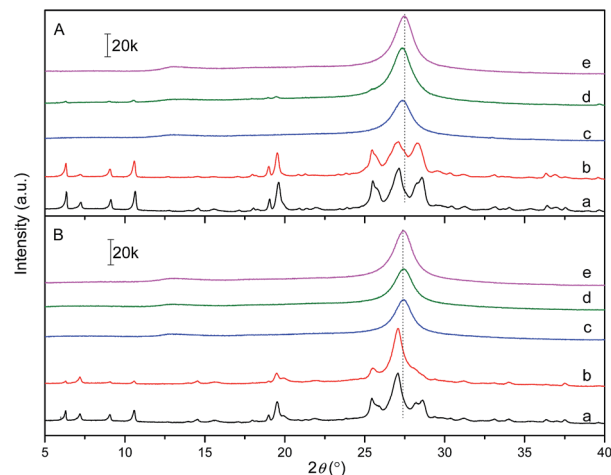


Fig. 1 XRD patterns of g-C₃N₄-T materials prepared without (A) and with (B) treatment of NaOH under different thermal treatment temperatures (a: 400; b: 425; c: 450; d: 475; and e: 500 °C).

preparation temperatures of g-C₃N₄, the complex peaks pertaining to melem disappeared while pronounced sharp peaks located at $2\theta = 27.4^\circ$ emerged, together with broad peaks with low intensity at $2\theta = 13^\circ$. The primary diffraction peaks were attributed to characteristic interplanar stacking structures of graphitic materials,²³ *i.e.* (002) planes with a d -spacing of *ca.* 0.325 nm. While the other minor peaks related to the in-plane structural packing motif, such as the hole-to-hole distance of the nitride pores in the crystal¹⁷ (Scheme 1), namely (100) planes. This means that, under higher temperatures above than 475 °C, the GndCl precursor transformed into g-C₃N₄. Additionally, the values of product mass of g-C₃N₄ powder (Table S1†), prepared using the same amount of GndCl, have also witnessed the further decomposition of the precursor under elevated temperatures.

In the case of g-C₃N₄-direct samples prepared using alkali treatment (Fig. 1B), under the low thermal treatment temperature of 400 °C, the XRD pattern of g-C₃N₄-400-NaOH showed very similar results with that of g-C₃N₄-400-direct. However, after the temperature was elevated slightly, it is of interest that an intensive peak at $2\theta = 27.2^\circ$ appeared on the pattern of g-C₃N₄-425-NaOH, which suggested the presence of graphitic-like crystalline generated on this material. However, on the other hand, the pattern of g-C₃N₄-425-direct still seemed like that of g-C₃N₄-400-direct, with no apparent diffraction associated with graphitic phase. Further raising temperature, the synthesized g-C₃N₄-NaOH materials revealed major diffraction peak at *ca.* 27.4°, resembling the results achieved on g-C₃N₄-direct specimens (Fig. 1A). By this comparison, it can be inferred that the treatment of NaOH for GndCl has effectively accelerated the condensation of melem units, allowing them to smoothly transform into graphitic layer of g-C₃N₄ even under relatively thermal treatment temperatures.

Fig. 2 depicts FT-IR spectra of g-C₃N₄ materials. For the g-C₃N₄ materials synthesized under 400–425 °C, two insensitive peaks at 3342 and 3130 cm⁻¹ have been observed, corresponding to the stretching modes of residual -NH₂ attached to

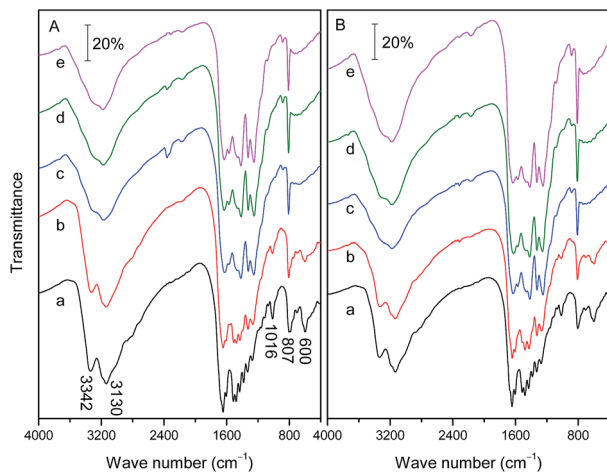


Fig. 2 FT-IR spectra of g-C₃N₄-T-direct (A) and g-C₃N₄-T-NaOH (B) materials under various thermal treatment temperatures (a: 400; b: 425; c: 450; d: 475; and e: 500 °C).

the sp² hybridized carbon, and -NH groups at the defect sites of the aromatic ring, respectively.⁴³ The dominating multiple bands in the 1600–1200 cm⁻¹ dominating were attributed to stretching and rotation vibration of C–N and C=N in heterocycles.⁴² Also, a sharp peak centered at 807 cm⁻¹ has been found for the spectrum of each sample, characteristic breathing mode of the triazine functionalities.⁴² In addition, there were two weak signals observed at 1016 and 600 cm⁻¹. The two peaks ought to be due to the uncompleted condensed intermediates of the GndCl precursor, which have also been previously reported by other groups.^{41,44} Whereas, as the thermal treatment temperature of GndCl was increased, the acquired FT-IR spectra showed remarkable variation. Wherein, the bands related to residual -NH₂ groups and uncondensed intermediates became weaker above 450 °C, while intensity of the band at 807 cm⁻¹ seemed to be improved and much sharper. Obviously, the change resulted from the contribution of high-degree condensation of melem-like species to wider conjugated graphitic layer at elevated temperatures. Consequently, the percentage of the free -NH₂ located at the edges of graphitic layers decreased.

The optical properties of the g-C₃N₄ samples were characterized by means of UV-vis DRS. The representative spectra obtained over g-C₃N₄-450 and g-C₃N₄-475 are given in Fig. 3. It can be seen that all the materials exhibited strong light absorption with edges at around 450 nm, which was derived from bandgap (*ca.* 2.75 eV) between HOMO and LUMO in the polymeric melon units of g-C₃N₄.²⁰ When the temperature was increased from 450 to 475 °C, the absorption edge was moved towards longer wavelength; the phenomenon has been detected on samples prepared both with and without alkali treatment. The red shift originated from the extension of electron delocalization in the conjugated layers of g-C₃N₄ with enhanced structural condensation.^{45,46} Compared with those of the pristine g-C₃N₄-direct samples, the UV-vis spectra of g-C₃N₄-NaOH materials showed absorption edges with much longer wavelengths. The comparison confirms that, the treatment of NaOH

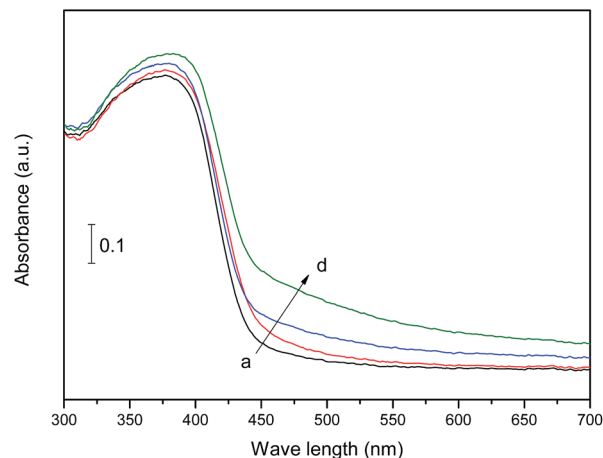


Fig. 3 UV-vis spectra of g-C₃N₄-450-direct (a), g-C₃N₄-475-direct (b), g-C₃N₄-450-NaOH (c), and g-C₃N₄-475-NaOH (d) materials.

has reinforced the condensation of g-C₃N₄ planar packing, in concert with the above XRD and FT-IR characterization results.

The chemical environment of C atoms in g-C₃N₄ samples was further investigated by ¹³C MAS NMR (Fig. 4). For the g-C₃N₄-direct samples prepared *via* direct thermal treatment, there were two apparent resonances detected for each spectrum. The peak with much higher intensity at δ = 164 ppm was assigned to the carbon atoms (C_α) connected with -NH₂ groups, whereas the other resonance at δ = 156 ppm was associated with carbon species in heptazine units and linked with bridging N atoms (C_β).^{45,47} These assignments are in good agreement with those of bulk g-C₃N₄ reported elsewhere,⁴⁷ further indicating the g-C₃N₄-direct materials were composed by heptazine tectonic units. Similarly, the spectra of g-C₃N₄-NaOH materials presented two signals at the same position. By comparison, the overall intensity of resonance peaks acquired on g-C₃N₄-NaOH samples was much stronger than those obtained in g-C₃N₄-direct samples, indicating that the former materials possessed a higher degree

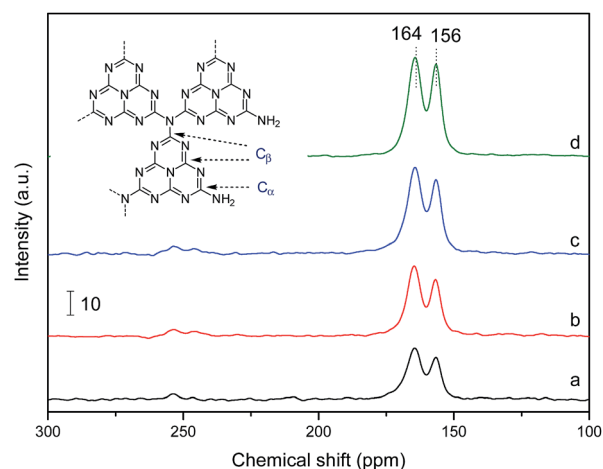


Fig. 4 Solid-state ¹³C NMR spectra of g-C₃N₄-450-direct (a), g-C₃N₄-475-direct (b), g-C₃N₄-450-NaOH (c), and g-C₃N₄-475-NaOH (d) materials.

of condensation of melon units. Moreover, the intensity ratio of peak at 156 ppm to 164 ppm seemed to be obviously enhanced from g-C₃N₄-475-direct to g-C₃N₄-475-NaOH. The finding proves that, at the same thermal treatment temperatures of GndCl, the aid of NaOH treatment favorably resulted in further condensation of melon units in g-C₃N₄ materials.

The bulk chemical composition of g-C₃N₄ materials was determined by EA measurement. As summarized in Table 1, the bulk molar ratios C/N of for the four g-C₃N₄-direct specimens were in the range of 0.64–0.66, lower than the theoretical value (0.75) of ideal g-C₃N₄ compound. Not surprisingly, during the thermal condensation procedures from GndCl to g-C₃N₄, the melon and/or melon intermediates could not be totally condensed, thereby leaving a certain amount of uncondensed primary and secondary amino group at the edges of graphitic layers.⁴⁸ XPS technique was subsequently applied to study the surface chemical composition of the materials. All the survey spectra (Fig. S1†) showed two sharp peaks centered at 288 and 398 eV, which were assigned to C 1s and N 1s signals, respectively. No apart from the two main elements, a minor peak at 532 eV could also be observed for each XPS survey, due to the trace water adsorbed on the surface. It is worth noting that there was no Cl signal (Cl 2s 265–285 eV) detected, indicating that there was no residual Cl element derived from GndCl precursor.

According to the peak areas of XPS surveys, chemical composition for each sample has been calculated (Table 1). The C/N molar ratios of on the surface were 0.70–0.75, superior to the values measured by EA. In our previous work,²⁵ we ascribed the gap to the considerable but inevitable loss of N species occurring on the surface of g-C₃N₄ in the thermal treatment stage. Further comparing the resultant formulas of the four samples, it can be found that the detailed C/N molar ratios of both surface and bulk phase, were very sensitive to the preparation conditions. That is, using either higher thermal treatment temperature or alkali treatment could prominently increase the percentage of C atoms. Unequivocally, as discussed above, the two procedures enabled further condensation of melon and/or melon fragments by eliminating the terminal amino groups, and eventually increased the total proportion of C atoms. On the other hand, owing to the deep condensation, much larger amount of small molecules (such as NH₃) released correspondingly. This is also responsible for the fact that the surface areas along with pore volumes (Table S2†) of g-C₃N₄ materials (Fig. S2† for their corresponding N₂ adsorption–desorption isotherms) showed

a noticeable improvement subjected to thermal treatment with high temperature or alkali treatment.

Since it is widely recognized that there exist several types of N species in g-C₃N₄, in order to probe the detailed information of N species of the present g-C₃N₄ materials, deconvolution of N 1s spectra of g-C₃N₄-475-direct and g-C₃N₄-475-NaOH has been further carried out. As shown in Fig. 5, the N 1s spectra of both the two samples could be separated into three species. The primary peaks with a binding energy of ca. 398.8 eV were assigned to sp²-hybridized N atoms with a bonding type as C=N–C in heptazine rings.¹⁷ These N atoms contributed to a majority of the total N species in g-C₃N₄-direct and g-C₃N₄-NaOH. The peak located at 400.1 eV were ascribed to sp² N atoms bonded to three atoms (*i.e.* C–N(–C)–C or C–N(–H)–C).⁴⁹ Such kind of N atoms, especially tertiary N, is a key junction that bridges two or three heptazine rings (Scheme 1). It should be also noted that the bridging N atoms have been regarded as the active base sites in base-mediated reactions, including CO₂-activating reactions⁵⁰ and transesterification reactions⁴⁶ since they possess higher basic intensity than other N species. The last peak with the highest binding energy corresponded to sp³ N atoms, *i.e.* free primary (–NH₂) and secondary (–NH–) amino groups at the edges of planar layers of g-C₃N₄.⁴⁹ In addition, a broad peak centered at 404.3 eV with a low intensity has also been detected at each N 1s spectrum (not shown here for concise), which was generally contributed to the charging effect of XPS.¹⁷

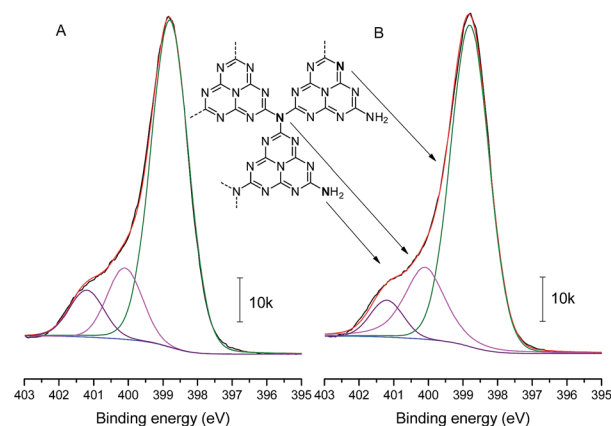


Fig. 5 N 1s spectra of g-C₃N₄-475-direct (A) and g-C₃N₄-475-NaOH (B).

Table 1 Bulk and surface chemical compositions and formulas of g-C₃N₄ samples

Sample	EA				XPS			
	C ^a	N ^a	H ^a	Formula	C ^b	N ^b	O ^b	Formula
g-C ₃ N ₄ -450-direct	32.50	58.76	2.607	C _{0.645} NH _{0.621}	40.05	57.75	2.20	C _{0.694} NO _{0.038}
g-C ₃ N ₄ -475-direct	33.71	59.20	2.494	C _{0.664} NH _{0.590}	41.49	56.02	2.49	C _{0.741} NO _{0.044}
g-C ₃ N ₄ -450-NaOH	32.45	58.37	2.567	C _{0.648} NH _{0.616}	40.32	56.81	2.87	C _{0.710} NO _{0.051}
g-C ₃ N ₄ -475-NaOH	33.04	58.23	2.402	C _{0.661} NH _{0.577}	41.60	55.12	3.28	C _{0.755} NO _{0.060}

^a Values expressed by weight percents. ^b Values expressed by molar percents.

According to the areas of deconvoluted peaks, the component distributions of various N atoms have been calculated and listed in Table 2. The percentages of sp^2 N bonded as C=N-C groups achieved on g-C₃N₄-475-direct and g-C₃N₄-475-NaOH were very close, implying that the two samples had similar population of heptazine rings on the surface area. In the cases of percentages of other types of N species, there were remarkable differences between the two solids. The N atoms bonded to three atoms accounted for 20.3% on g-C₃N₄-475-NaOH, comparatively higher than those of g-C₃N₄-475-direct, whereas g-C₃N₄-475-NaOH owned much less sp^3 N atoms than its counterpart. By the comparison, it can be verified that, the melem and melon-like fragments which have abundant terminal amino groups, underwent co-condensation of higher degree on g-C₃N₄-475-NaOH than g-C₃N₄-475-direct, thus yielding greater proportion of tertiary bridging N species on g-C₃N₄-475-NaOH.

Since the above findings in several characterization techniques have unanimously confirmed the induction of NaOH could finally improve the degree of condensation of g-C₃N₄, it is of interest to elucidate the interaction between the GndCl precursor and NaOH. Either GndCl or NaOH is easily to be dissolved in ethanol. However, after the contact of the two ethanolic solutions, as expressed in the Experimental section, white precipitation has been clearly observed. By the analysis of XRD characterization (Fig. S3†), it was proved that such a white solid was pure NaCl (PDF #05-0628). Regarding the possible

NaOH remaining in the final g-C₃N₄-NaOH materials, it should be noted that, the molar amount of NaOH was 0.025 mol, much less than the value of GndCl (0.094 mol). According to the possible reaction route (GndCl + NaOH → GndOH + NaCl), such NaOH would be totally converted into NaCl. On the other hand, according to the XRD patterns (Fig. 1) and XPS survey (Fig. S1†) of g-C₃N₄-NaOH materials (e.g. g-C₃N₄-450-NaOH), there is no obvious diffraction peaks associated with NaCl (PDF #05-0628), or any signal of Na 1s (1086–1072 eV) or Cl 2s (265–285 eV), respectively. Therefore, it can be confirmed that NaOH has been totally reacted with GndCl, and there was no residual NaOH existing in the final g-C₃N₄-NaOH materials.

Moreover, if mixing ethanolic solutions of GndCl and KOH, white precipitation, namely KCl (PDF #41-1476), was also obtained (Fig. S3†). Because either NaCl or KCl is hardly dissolved in ethanol, we surmised that, GndCl and NaOH reacted under ethanolic solution, and generated NaCl and guanidine-hydroxide-like compound (GndOH), as illustrated in Scheme 2. On the other hand, as we reported previously, GndCl could be transformed into g-C₃N₄ subjected to four-step polycondensation.⁴⁸ Likewise, GndOH containing guanidine group should be smoothly converted into g-C₃N₄ after the same thermal treatment procedure as GndCl. Additionally, we think that the presence of hydroxide anions accelerated the condensation of melem and melon fragments to the ultimate planar graphitic polymer of g-C₃N₄. Thereby, it can be well understood why g-C₃N₄-NaOH sample possessed higher amount of bridging N atoms yet lower amount of terminal amines than g-C₃N₄ under the same thermal treatment temperatures. Indeed, such similar effect of alkali compounds has also been reported in the work involving the synthesis or posttreatment of g-C₃N₄ materials.^{19,51}

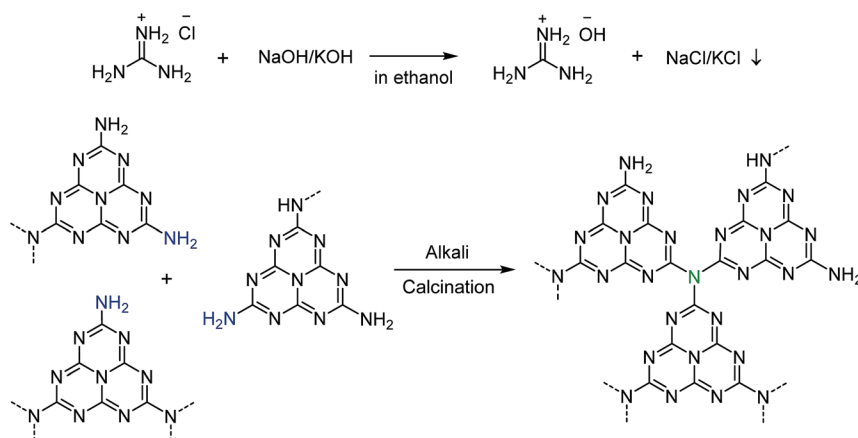
Table 2 Distributions of various N species for g-C₃N₄ materials^a

Sample	Percentage of N components (mol%)		
	401.2 eV -NH ₂	400.1 eV C-N(-C)-C	398.8 eV C=N-C
g-C ₃ N ₄ -475-direct	9.9	14.8	75.3
g-C ₃ N ₄ -475-NaOH	6.0	20.3	73.7

^a Determined by N 1s XPS profiles.

3.2. Catalyst activity

The g-C₃N₄ materials prepared without and with alkali assistant were applied as catalysts to evaluate their activity in the cycloaddition reactions of CO₂ to PO (Table 3). Initially, a blank test without any catalyst was performed and the corresponding conversion of PO was less than 3% (entry 1). Also, the catalytic activity acquired under either ZnI₂ (entry 2) or bare g-C₃N₄



Scheme 2 A possible mechanism of alkali-assisted synthesis of g-C₃N₄-MOH.

Table 3 Catalytic performances various g-C₃N₄ samples in cycloaddition reactions of CO₂ to PO^a

Entry	Catalyst	Conv. (%)	Sel. (%)	Yield (%)
1	—	2.5	95.2	2.4
2	ZnI ₂ ^b	12.8	94.9	12.1
3	g-C ₃ N ₄ -450-direct ^c	3.0	97.2	3.7
4	g-C ₃ N ₄ -450-direct	58.3	99.7	58.1
5	g-C ₃ N ₄ -475-direct	60.6	99.8	60.5
6	g-C ₃ N ₄ -500-direct	65.2	99.5	64.9
7	g-C ₃ N ₄ -525-direct	79.6	99.6	79.3
8	g-C ₃ N ₄ -550-direct	82.1	99.6	81.8
9	g-C ₃ N ₄ -450-NaOH ^c	3.8	97.4	3.7
10	g-C ₃ N ₄ -450-NaOH	79.9	99.1	79.2
11	g-C ₃ N ₄ -475-NaOH	90.0	99.4	89.5
12	g-C ₃ N ₄ -500-NaOH	92.6	99.4	92.0

^a Reaction conditions: $V_{\text{PO}} = 10$ mL, $p_{\text{CO}_2} = 2.0$ MPa, $T = 140$ °C, and $t = 6$ h. Unless specified, each entry was added with 0.4 g of g-C₃N₄ and 38 mg of ZnI₂. ^b Without g-C₃N₄. ^c Without ZnI₂.

(entries 3 and 9) was very poor. By contrast, after addition of g-C₃N₄ and ZnI₂ into the reaction (entry 4), the catalytic productivity was remarkably improved, affording a PO conversion of 58.3% along with a high selectivity to PC. This means that there was a potential synergy between g-C₃N₄ and ZnI₂ for the catalytic cycloaddition of CO₂ with PO (discussed below).

With elevating the thermal treatment temperatures of GndCl (entries 4–8), the final g-C₃N₄-direct materials exhibited a monotonous increase in terms of the PO conversions. Wherein, g-C₃N₄-550-direct sample offered the highest PC yield as much as 82% (entry 8). As mentioned above, there exist at least three types of N species in g-C₃N₄. Among them, it has been widely recognized the bridging tertiary amine that connects the heptazine rings has superior basic intensity to other free amino groups (*i.e.* uncondensed primary and secondary amines located at the graphitic layer of g-C₃N₄).^{39,50} During the transformation of GndCl to g-C₃N₄, high thermal treatment temperatures would favor the further condensation of oligomeric melon species by releasing small molecules such as NH₃. Consequently, the amount of tertiary amines has been improved, thus facilitating the whole activity in activating CO₂ molecules. Interestingly, under the same reaction conditions, the g-C₃N₄-NaOH materials synthesized under lower temperatures but with the alkali assistant also demonstrated high catalytic activity (entries 10–12); the PO conversion received were in the range of 79.9–92.6%. Indeed, if compared based on the same thermal treatment temperatures, the activity acquired over g-C₃N₄-NaOH, for instance g-C₃N₄-475-NaOH (90.0%), was much higher than that of its simple counterpart (g-C₃N₄-475-direct, 60.6%). As proved in FT-IR and XPS, the aid of NaOH effectively induced further polymerization of the original uncondensed melon-like fragments. In this sense, the threshold temperature for higher polymerized g-C₃N₄ compound has been reduced; therefore even under low thermal treatment temperatures, g-C₃N₄ materials with high amounts of important basic trigonal N atoms could be favorably synthesized.

In order to optimize reaction conditions and thus obtain high PC productivity, the effects of reaction conditions on the catalytic performances have been subsequently investigated using g-C₃N₄-475-NaOH as a reference catalyst. As depicted in Fig. 6A, using more amounts of catalyst could effectively bring out a progressive increase of catalytic activity; however the PO conversion leveled off when the weight of catalyst was above 0.4 g. Also, the catalytic performance was found to be dependent on reaction temperature (Fig. 6B). Under the low temperatures (100–110 °C), the activity was very poor. Meanwhile, the corresponding selectivity was lower than 80%, mainly owing to the hydrolysis of PO to propylene glycol (PG) in the presence of residual water in the reactor. Further raising the temperature resulted in drastic improvements in both PO conversion and PC selectivity. Although the PC yield could be achieved as *ca.* 93% at 150 °C; however considering the reaction economy, 140 °C was selected as the optimal temperature. In addition to catalyst amount and reaction temperature, the catalytic performances under various CO₂ pressures and reaction time have been also evaluated. The use of higher CO₂ pressures could clearly improve the catalytic activity (Fig. 6C). Instead, excessive CO₂ pressures resulted in a regressive PO conversion. This is probably because under that harsh circumstance, acidic CO₂ might dissolve in PO and then generate strong CO₂-PO complex.⁵² Additionally, it was found that, after 6 h of reaction time, the catalytic activity presented no apparent increase (Fig. S4†).

Besides, recyclability and reproductivity is also an important issue to examine a heterogeneous catalyst. Taking into account this point, a series of consecutive catalytic tests have been carried out over g-C₃N₄-475-NaOH, on the basis of the above optimized reaction conditions. As presented in Fig. 7, during the repetitious five runs, the selectivities to PC were all higher than 99%. Simultaneously, it is observed that the catalytic conversion of PO underwent no apparent decline within the successive experiments. Furthermore, XRD patterns and FT-IR characterization results (Fig. S5†) of the spent g-C₃N₄-475-NaOH catalysts exhibited the same profiles as the fresh one. On the other hand, for those mesoporous g-C₃N₄ materials either loaded with transition metal halides or functionalized with quaternary amines reported by us,^{37,38} they all showed apparent decrease in catalytic activity in the initial several runs, mainly because they possessed a certain amount of uncondensed fragments that were liable to leach in liquid phase. Hence, given the fact, it is proved that the present g-C₃N₄-NaOH catalysts are relatively stable heterogeneous catalysts.

As NaOH can be utilized to induce the polymerization of g-C₃N₄ under relatively low thermal treatment temperatures. In this work, we have also tentatively introduced KOH into the preparation routes of g-C₃N₄ material, and produced g-C₃N₄-475-KOH. The corresponding XRD pattern and FT-IR spectrum (Fig. S6†) of the sample are in the same as that of g-C₃N₄-475-NaOH, with no apparent diffraction lines indexed as KCl compound. The catalytic performance for the cycloaddition of CO₂ was tested thereafter. As summarized in Table 4, the synthesized g-C₃N₄-475-KOH sample exhibited high PO conversions along with high selectivities to the desired PC. Besides PO, the catalytic tests using ethylene oxide and

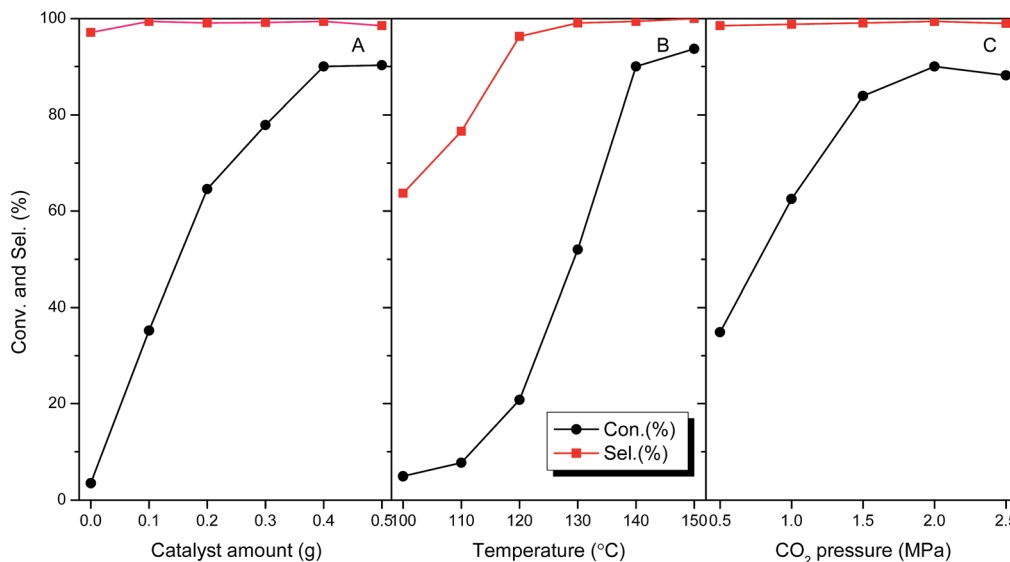


Fig. 6 Effects of reaction conditions on the catalytic performances of $g\text{-C}_3\text{N}_4\text{-475-NaOH}$ in cycloaddition reactions of CO_2 . All the data were collected at 6 h. Reaction conditions: $V_{\text{PO}} = 10$ mL and 38 mg of ZnI_2 added. (A) $p_{\text{CO}_2} = 2.0$ MPa and $T = 140$ °C. (B) $W_{\text{catal.}} = 0.4$ g and $p_{\text{CO}_2} = 2.0$ MPa. (C) $W_{\text{catal.}} = 0.4$ g and $T = 140$ °C.

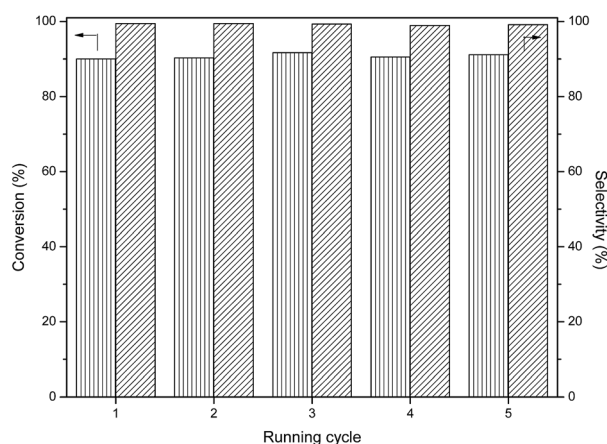


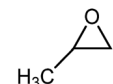
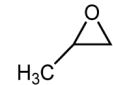
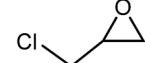
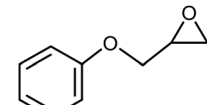
Fig. 7 Recycling tests for $g\text{-C}_3\text{N}_4\text{-475-NaOH}$ in the cycloaddition reactions of CO_2 . Reaction conditions: $V_{\text{PO}} = 10$ mL, $p_{\text{CO}_2} = 2.0$ MPa, $T = 140$ °C, $t = 6$ h, $W_{\text{catal.}} = 0.4$ g and 38 mg of ZnI_2 added.

chloropropylene oxide as substrates also demonstrated high-performance catalytic results under identical reaction conditions. Therein, it can be inferred that the present alkali-assisted synthetic approach is a versatile and practical strategy for the fabrication of high-performance $g\text{-C}_3\text{N}_4$ materials for the catalytic synthesis of cyclic carbonates from cycloaddition of CO_2 to epoxides.

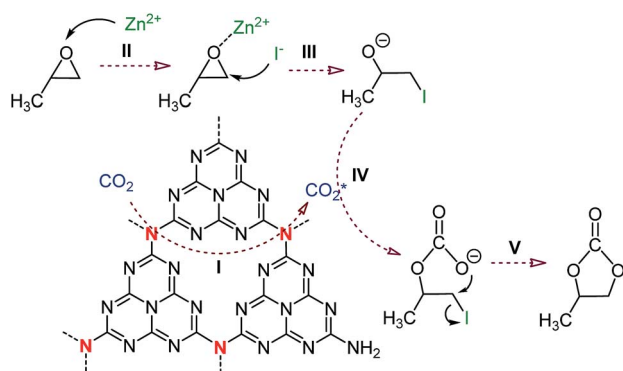
According to the characterization and catalytic results in this study as well as other related work,^{52,53} a possible mechanism for cycloaddition of CO_2 catalyzed by $g\text{-C}_3\text{N}_4$ was proposed, as described in Scheme 3. Compared with the uncondensed terminal amino groups at the edges of graphitic layers of $g\text{-C}_3\text{N}_4$, bridging tertiary N atoms possessed higher intensity of basicity. Therefore, for an acidic CO_2 molecule, it is preferentially adsorbed and then activated by the tertiary N atoms (Step

I). On the other hand, as suggested by Dai *et al.*⁵⁴ the amino groups of $g\text{-C}_3\text{N}_4$ were able to adsorb oxygen-containing small molecules, such as cycloalkene oxide, *via* hydrogen bonds. Therefore, we surmise that PO could also be adsorbed and activated by the graphitic edges of $g\text{-C}_3\text{N}_4$. Additionally, Zn^{2+} cation coordinated with oxygen atom of PO and thus triggered the polarization of C–O bonds (Step II). Next, a carbon atom of PO was attacked by I^- anion, leading to a ring opening and generating an iodoalkoxy anion (Step III).³⁷ After that, the

Table 4 Catalytic performance of a series of $g\text{-C}_3\text{N}_4$ materials prepared using various alkali compounds^a

Catalyst	Epoxide	Conv. (%)	Sel. (%)	Yield (%)
$g\text{-C}_3\text{N}_4\text{-475-NaOH}$		90.0	99.4	89.5
$g\text{-C}_3\text{N}_4\text{-475-KOH}$		91.7	99.1	90.9
$g\text{-C}_3\text{N}_4\text{-475-NaOH}$		92.3	99.5	91.8
$g\text{-C}_3\text{N}_4\text{-475-NaOH}$		86.4	99.2	85.7
$g\text{-C}_3\text{N}_4\text{-475-NaOH}$		83.1	99.0	82.3

^a Reaction conditions: $V_{\text{epoxide}} = 10$ mL, $p_{\text{CO}_2} = 2.0$ MPa, $T = 140$ °C, $t = 6$ h, $W_{\text{catal.}} = 0.4$ g, and 38 mg of ZnI_2 added.



Scheme 3 A possible reaction pathway for cycloaddition of CO₂ catalyzed by g-C₃N₄.

iodoalkoxy anion reacted with the activated CO₂ molecule on the surface of g-C₃N₄, yielding a linear iodocarbonate anion (Step IV). Finally, the anion intermediate transformed into PC through a ring closing process (Step V). In a short summary, the role of ZnI₂ was solely to activate epoxide by inducing its ring opening, while g-C₃N₄ took in charge of adsorbing and then activating CO₂ by N-containing basic sites. With this hypothetical mechanism, it can be well explained why with ZnI₂ or g-C₃N₄ alone, the corresponding catalytic activity was limited. Once again, because g-C₃N₄-NaOH and g-C₃N₄-KOH owned more proportion of crucial bridging N species than g-C₃N₄-direct, the former naturally offered higher catalytic activity than the latter.

As stated above, owing to their abundant N-containing species, g-C₃N₄ materials have been applied as catalysts in many CO₂-activating reactions. Therefore, it would be of interest to compare the catalytic performances offered by the present g-C₃N₄ samples with those of previously reported

g-C₃N₄ materials. Given this point, we summarize the catalytic results of various g-C₃N₄ materials in the cycloaddition of CO₂ with PO in Table 5. To the best of our knowledge, all the reported g-C₃N₄-based catalysts have been covered. Because the reaction conditions (including catalyst amount, reaction time, and PO feeding volume) deviate from each other whereas the reaction temperatures adopted are *ca.* 140 °C, for a fair comparison, TOF value (based on g-C₃N₄ component) has been calculated for each entry. As listed in Table 5, the most efficient one is g-C₃N₄ catalyst supported on mesoporous SBA-15 (entry 2), followed by mesoporous g-C₃N₄ materials functionalized by quaternary ammonium (entry 3) and loaded with ZnBr₂ (entry 4). It is worth noting that such materials (also including entry 1) were prepared using mesoporous silicas as catalytic supports or sacrificial templates, which demanded time-consuming and complicated procedures. Also, the soft templates (*i.e.* pluronic surfactant) applied for the mesoporous silicas are relatively expensive. In sharp contrast, the present g-C₃N₄ catalysts were prepared *via* a much more convenient way, however also showing pretty good catalytic activities. Furthermore, the feeding amount of PO is 10 mL (entries 6–7), comparatively higher than other values. In addition to g-C₃N₄-based materials, the catalytic performances of some heterogeneous catalysts have also been provided in Table 5. Entries 8–11 are typical ionic liquids catalyst immobilized on various solids, including graphene oxide sheets, silica gel, and cross-linked polymer. The active sites of these catalysts were solely halide anions, and the TOF values acquired them were in the range of 2 to 8.8 h⁻¹ (note: the catalyst amount for each entry was based on the total catalyst). As noted above, the preparation of such grafted IL catalyst was very complicated and also demanded expensive silicane-type coupling agents. Also the activity of MFI-type zeolite containing I⁻ is also lower than that of g-C₃N₄-475-

Table 5 Comparison of the catalytic performances of various g-C₃N₄-based materials and other heterogeneous catalysts in cycloaddition of CO₂ with PO

Entry	Catalyst	<i>T</i> (°C)	<i>t</i> (h)	<i>V</i> _{PO} (mL)	<i>W</i> _{catal.} (mg)	Yield (%)	TOF ^k (h ⁻¹)
1 ^{a24}	MS-MCN	140	10	1.5	20	30.6	3.3
2 ^{b39}	g-C ₃ N ₄ /SBA-15	150	1.5	3	100	96.1	28.1
3 ^{c38}	<i>n</i> -ButBr/mp-C ₃ N ₄	140	6	10	200	87.7	10.7
4 ^{d37}	ZnBr ₂ /mp-C ₃ N ₄	140	6	7	200	98.9	8.4
5 ^{e50}	u-g-C ₃ N ₄ -480	130	4	1.5	50	23.7	2.6
6	g-C ₃ N ₄ -475-NaOH	140	6	10	400	89.5	5.4
7	g-C ₃ N ₄ -475-KOH	140	6	10	400	90.9	5.5
8 ^{f15}	GO-[SmIm]I	140	4	15	600	96	8.8
9 ^{g55}	PDDA-Br-ZnBr ₂ -2/SiO ₂	100	5	0.7	100	96.7	2.0
10 ^{h5}	P-DVB-HEImBr	140	5	2	200	93.2	2.7
11 ⁱ⁶	PS-DHPIMBr	130	3	1.75	200	96.0	4.1
12 ^{j56}	LMFI-I	140	4	0.7	100	97.1	2.5

^a Prepared using disk-shaped 2D hexagonal mesoporous silica as a hard template and melamine as a precursor. ^b Prepared using SBA-15 as a catalytic support and dicyandiamide as a precursor through a chemical-vapor-deposition method. Zn²⁺ was further doped into g-C₃N₄/SBA-15 as an additive. ^c Prepared using silica nanoparticles as hard templates and cyanamide as a precursor. The synthesized mp-C₃N₄ was grafted with *n*-bromobutane. ^d ZnBr₂ supported on mp-C₃N₄ material. ^e Prepared using urea as a starting material without addition of any template. ^f Graphene oxide sheets immobilized with functionalized imidazolium ionic liquid with iodide ion. ^g Polymeric quaternary ammonium salt supported on silica gel. ^h Cross-linked polymer grafted with functionalized ionic liquid with bromide ion. ⁱ Polystyrene supported with diol functionalized ionic liquids. ^j Organic-inorganic hybrid zeolites with the MFI-type lamellar structure. ^k The detailed calculation method for TOF was expressed in the Experimental section.

MOH catalyst under the same reaction conditions. Hence, in viewpoint of both catalyst preparation and catalytic activity, the present g-C₃N₄ materials could serve potential heterogeneous catalysts for efficient cycloaddition of CO₂.

4. Conclusion

In summary, we have developed a facile and fast strategy to fabricate g-C₃N₄ materials. The using of NaOH or KOH could effectively reduce the threshold temperatures of the formation of g-C₃N₄, enabling GndCl to be smoothly converted into g-C₃N₄ at 450–475 °C. Due to the condensation with a higher level, the g-C₃N₄-NaOH materials had much more bridging tertiary N atoms than g-C₃N₄-direct samples. In the cycloaddition of CO₂ to PO, both g-C₃N₄-NaOH and g-C₃N₄-KOH samples showed good catalytic performances, higher than the results received over g-C₃N₄-direct sample under the same reaction conditions. Meanwhile, the g-C₃N₄-NaOH can be reused for at least five times without any loss of catalytic activity. Compared with other mesoporous and supported g-C₃N₄ materials, the present g-C₃N₄ samples were synthesized with an easier method, while manifesting a promising catalytic application for the cycloaddition of CO₂ to PC.

Acknowledgements

This work was supported by National Natural Science Foundation of China (21203014 and 21376032), Jiangsu Key Laboratory of Advanced Catalytic Materials and Technology (BM2012110), and the Project Funded by the Priority Academic Program Development of Jiangsu Higher Education Institutions.

Notes and references

- J. Roeser, K. Kailasam and A. Thomas, *ChemSusChem*, 2012, **5**, 1793–1799.
- M. North, R. Pasquale and C. Young, *Green Chem.*, 2010, **12**, 1514–1539.
- J. Ma, N. Sun, X. Zhang, N. Zhao, F. Xiao, W. Wei and Y. Sun, *Catal. Today*, 2009, **148**, 221–231.
- W.-L. Dai, S.-L. Luo, S.-F. Yin and C.-T. Au, *Appl. Catal., A*, 2009, **366**, 2–12.
- W.-L. Dai, B. Jin, S.-L. Luo, S.-F. Yin, X.-B. Luo and C.-T. Au, *J. CO₂ Util.*, 2013, **3–4**, 7–13.
- R. A. Watile, K. M. Deshmukh, K. P. Dhake and B. M. Bhanage, *Catal.: Sci. Technol.*, 2012, **2**, 1051–1055.
- A. Ion, V. Parvulescu, P. Jacobs and D. De Vos, *Appl. Catal., A*, 2009, **363**, 40–44.
- J.-Q. Wang, J. Sun, W.-G. Cheng, C.-Y. Shi, K. Dong, X.-P. Zhang and S.-J. Zhang, *Catal.: Sci. Technol.*, 2012, **2**, 600–605.
- X.-Y. Liu, L.-B. Sun, X.-D. Liu, A.-G. Li, F. Lu and X.-Q. Liu, *ACS Appl. Mater. Interfaces*, 2013, **5**, 9823–9829.
- M. H. Anthofer, M. E. Wilhelm, M. Cokoja, I. I. Markovits, A. Pöthig, J. Mink, W. A. Herrmann and F. E. Kühn, *Catal.: Sci. Technol.*, 2014, **4**, 1749–1758.
- L. Han, H. Li, S.-J. Choi, M.-S. Park, S.-M. Lee, Y.-J. Kim and D.-W. Park, *Appl. Catal., A*, 2012, **429**, 67–72.
- X. Zhang, D. Wang, N. Zhao, A. S. Al-Arifi, T. Aouak, Z. A. Al-Othman, W. Wei and Y. Sun, *Catal. Commun.*, 2009, **11**, 43–46.
- W. Cheng, X. Chen, J. Sun, J. Wang and S. Zhang, *Catal. Today*, 2013, **200**, 117–124.
- S. Udayakumar, M.-K. Lee, H.-L. Shim, S.-W. Park and D.-W. Park, *Catal. Commun.*, 2009, **10**, 659–664.
- J. Xu, M. Xu, J. Wu, H. Wu, W.-H. Zhang and Y.-X. Li, *RSC Adv.*, 2015, **5**, 72361–72368.
- J. Xu, K.-Z. Long, Y. Wang, B. Xue and Y.-X. Li, *Appl. Catal., A*, 2015, **496**, 1–8.
- A. Thomas, A. Fischer, F. Goettmann, M. Antonietti, J.-O. Müller, R. Schlögl and J. M. Carlsson, *J. Mater. Chem.*, 2008, **18**, 4893–4908.
- Y. Gong, M. Li, H. Li and Y. Wang, *Green Chem.*, 2015, **17**, 715–736.
- J. Zhu, P. Xiao, H. Li and S. A. C. Carabineiro, *ACS Appl. Mater. Interfaces*, 2014, **6**, 16449–16465.
- X. Wang, K. Maeda, A. Thomas and K. Takanabe, *Nat. Mater.*, 2009, **8**, 76–80.
- F. Su, S. C. Mathew, G. Lipner, X. Fu, M. Antonietti, S. Blechert and X. Wang, *J. Am. Chem. Soc.*, 2010, **132**, 16299–16301.
- S. Cao, J. Low, J. Yu and M. Jaroniec, *Adv. Mater.*, 2015, **27**, 2150–2176.
- F. Goettmann, A. Fischer, M. Antonietti and A. Thomas, *Angew. Chem., Int. Ed.*, 2006, **45**, 4467–4471.
- M. B. Ansari, B.-H. Min, Y.-H. Mo and S.-E. Park, *Green Chem.*, 2011, **13**, 1416–1421.
- J. Xu, T. Chen, Q. Jiang and Y.-X. Li, *Chem.-Asian J.*, 2014, **9**, 3269–3277.
- Y. Zheng, J. Liu, J. Liang, M. Jaroniec and S. Z. Qiao, *Energy Environ. Sci.*, 2012, **5**, 6717–6731.
- S. S. Park, S.-W. Chu, C. Xue, D. Zhao and C.-S. Ha, *J. Mater. Chem.*, 2011, **21**, 10801–10807.
- Q. Li, J. Yang, D. Feng, Z. Wu, Q. Wu, S. S. Park, C.-S. Ha and D. Zhao, *Nano Res.*, 2010, **3**, 632–642.
- F. Su, M. Antonietti and X. Wang, *Catal.: Sci. Technol.*, 2012, **2**, 1005–1009.
- S. N. Talapaneni, S. Anandan, G. P. Mane, C. Anand, D. S. Dhawale, S. Varghese, A. Mano, T. Mori and A. Vinu, *J. Mater. Chem.*, 2012, **22**, 9831–9840.
- J. Xu, K. Shen, B. Xue and Y.-X. Li, *J. Mol. Catal. A: Chem.*, 2013, **372**, 105–113.
- M. B. Ansari, H. Jin, M. N. Parvin and S.-E. Park, *Catal. Today*, 2012, **185**, 211–216.
- J. Xu, T. Chen, X. Wang, B. Xue and Y.-X. Li, *Catal.: Sci. Technol.*, 2014, **4**, 2126–2133.
- X. Jin, V. V. Balasubramanian, S. T. Selvan, D. P. Sawant, M. A. Chari, G. Q. Lu and A. Vinu, *Angew. Chem., Int. Ed.*, 2009, **48**, 7884–7887.
- F. Goettmann, A. Thomas and M. Antonietti, *Angew. Chem., Int. Ed.*, 2007, **46**, 2717–2720.
- D.-H. Lan, H.-T. Wang, L. Chen, C.-T. Au and S.-F. Yin, *Carbon*, 2016, **100**, 81–89.

- 37 J. Xu, F. Wu, Q. Jiang, J.-K. Shang and Y.-X. Li, *J. Mol. Catal. A: Chem.*, 2015, **403**, 77–83.
- 38 J. Xu, F. Wu, Q. Jiang and Y.-X. Li, *Catal.: Sci. Technol.*, 2015, **5**, 447–454.
- 39 Z. Huang, F. Li, B. Chen, T. Lu, Y. Yuan and G. Yuan, *Appl. Catal., B*, 2013, **136**, 269–277.
- 40 S. Chu, C. Wang, J. Feng, Y. Wang and Z. Zou, *Int. J. Hydrogen Energy*, 2014, **39**, 13519–13526.
- 41 L. S. Rangel, J. R. de la Rosa, C. J. L. Ortiz and M. J. Castaldi, *J. Anal. Appl. Pyrolysis*, 2015, **113**, 564–574.
- 42 M. J. Bojdys, J.-O. Müller, M. Antonietti and A. Thomas, *Chem.–Eur. J.*, 2008, **14**, 8177–8182.
- 43 E. Z. Lee, Y.-S. Jun, W. H. Hong, A. Thomas and M. M. Jin, *Angew. Chem., Int. Ed.*, 2010, **49**, 9706–9710.
- 44 L. Shi, L. Liang, F. Wang, J. Ma and J. Sun, *Catal.: Sci. Technol.*, 2014, **4**, 3235–3243.
- 45 Q. Gu, Y. Liao, L. Yin, J. Long, X. Wang and C. Xue, *Appl. Catal., B*, 2015, **165**, 503–510.
- 46 J. Xu, Y. Li, S. Peng, G. Lu and S. Li, *Phys. Chem. Chem. Phys.*, 2013, **15**, 7657–7665.
- 47 Y. Cui, Z. Ding, X. Fu and X. Wang, *Angew. Chem., Int. Ed.*, 2012, **51**, 11814–11818.
- 48 J. Xu, H.-T. Wu, X. Wang, B. Xue, Y.-X. Li and Y. Cao, *Phys. Chem. Chem. Phys.*, 2013, **15**, 4510–4517.
- 49 F. Dong, L. Wu, Y. Sun, M. Fu, Z. Wu and S. C. Lee, *J. Mater. Chem.*, 2011, **21**, 15171–15174.
- 50 Q. Su, J. Sun, J. Wang, Z. Yang, W. Cheng and S. Zhang, *Catal.: Sci. Technol.*, 2014, **4**, 1556–1562.
- 51 X. Bai, S. Yan, J. Wang, L. Wang, W. Jiang, S. Wu, C. Sun and Y. Zhu, *J. Mater. Chem. A*, 2014, **2**, 17521–17529.
- 52 L.-F. Xiao, F.-W. Li, J.-J. Peng and C.-G. Xia, *J. Mol. Catal. A: Chem.*, 2006, **253**, 265–269.
- 53 J. Sun, L. Wang, S. Zhang, Z. Li, X. Zhang, W. Dai and R. Mori, *J. Mol. Catal. A: Chem.*, 2006, **256**, 295–300.
- 54 J. Ding, Q. Liu, Z. Zhang, X. Liu, J. Zhao, S. Cheng, B. Zong and W.-L. Dai, *Appl. Catal., B*, 2015, **165**, 511–518.
- 55 B. Song, L. Guo, R. Zhang, X. Zhao, H. Gan, C. Chen, J. Chen, W. Zhu and Z. Hou, *J. CO₂ Util.*, 2014, **6**, 62–68.
- 56 C.-G. Li, L. Xu, P. Wu, H. Wu and M. He, *Chem. Commun.*, 2014, **50**, 15764–15767.